System Identification and Controller Optimization of a Coaxial Quadrotor UAV in Hover

Sung Hyeok Cho[1], and Subodh Bhandari[2]
California Polytechnic State University-Pomona, Pomona, CA

Frank C. Sanders[3]
San Jose Research Foundation, San Jose, CA

Kenny K. Cheung[4]
Universities Space Research Association, Moffett Field, CA, USA

and

Mark B. Tischler[5]
U.S. Army Aviation Development Directorate, Moffett Field, CA

With relatively little study done on the stability and control of coaxial multirotor UAV configurations, more data is required to accurately assess the benefits of the coaxial configuration compared to traditional multirotor configurations. In this paper, system identification of the 3DR X8+ aircraft, a coaxial quadrotor, via frequency domain system identification techniques were performed. The obtained dynamics were then used to design and optimize an Attitude Command/Attitude Hold control law utilizing the Explicit Model Following architecture. The results were compared with the results of a previously identified and optimized 3DR IRIS+, a quadrotor, with similar physical characteristics.

I. Nomenclature

ACAH	=	Attitude Command Attitude Hold
EMF	=	Explicit Model Following
Kv	=	Motor Velocity Constant
LiPo	=	Lithium-Polymer
mAh	=	Miliamp Hour
p	=	Roll Rate, rad/s
q	=	Pitch Rate, rad/s
r	=	Yaw Rate, rad/s
RMS	=	Root Mean Square
UAS	=	Unmanned Aerial System
δ_{col}	=	Bare Airframe Throttle Input
δ_{lat}	=	Bare Airframe Roll Input
δ_{lon}	=	Bare Airframe Pitch Input
δ_{ped}	=	Bare Airframe Yaw Input
θ	=	Pitch Angle, rad
τ	=	Time Delay, sec

[1] Undergraduate Student, Aerospace Engineering Department, and AIAA Student Member.
[2] Professor, Aerospace Engineering Department, and AIAA Associate Fellow.
[3] Aerospace Engineer, and AIAA Member.
[4] Aeroflightdynamics Technical Area Lead, and AIAA Senior Member.
[5] Flight Control Technology Group Leader, Senior Scientist, and AIAA Associate Fellow.

φ = Roll Angle, rad
ψ = Yaw Angle, rad

II. Introduction

The current surge in personal and commercial UAV development has led to various configurations of UAVs that deviate from the standard quadrotor configuration. While most configurations have been shown to be stable due the highly adaptable motor mixing and feedback control, relatively little research has been done on the effect of nonstandard configurations. Most private UAV operators utilize trial and error to tune the gains of the control system, which can often be time consuming and will not ensure optimal performance. Therefore, a method of identifying the dynamics of various configurations, as well as a standardized method of designing and optimizing control laws for unconventional configurations is critical for more efficient future development of multirotors, for both private and commercial usage.

This paper presents the identification of the hover/low-speed dynamics of a 3DR X8+ coaxial multirotor using the CIFER® (Comprehensive Identification from Frequency Responses) software package [1] and control law design and optimization using the CONDUIT® (Control Designer's Unified Interface) software package [2]. The identified model characteristics was compared with that of the IRIS+ in order to assess the effect of the unconventional coaxial configuration. In addition, the paper discusses the design of a control system using the identified model, optimization for gust rejection, and comparison of optimized control system with that of the IRIS+.

III. 3DR X8+ Test Vehicle

The aircraft tested was the 3DR X8+, a coaxial quadrotor, which is shown in Fig. 1. The vehicle was modified in order to facilitate data collection and flight testing. It is equipped with a PixHawk 2.1 flight controller, operating a modified ArduCopter firmware. The system logs angular rates, velocity estimations, attitudes, pilot input, and mixer input at 100 Hz. In addition, the system allows for injection of custom pilot inputs as well as mixer inputs, which is used for both system identification and turbulence rejection data collection. The physical properties of the 3DR X8+ is shown in Table 1.

Fig. 1 3DR X8+ multicopter.

Table 1 Physical Properties of X8+.

Characteristics	Value	Characteristics	Value
Dimensions	18.75” x 12” x 9”	Flight Controller	Pixhawk 2.1
Empty Weight	4.39 lb	Firmware	ArduCopter 3.5.1
Takeoff Weight	5.51 lb	Motor	880 Kv x 8
Propellers	11”	Configuration	X8

IV. Identification of Flight Dynamics Model

A. Flight Testing and Data Collection

The flight tests were conducted with the ArduCopter's stock "Stabilize" mode control system, with frequency sweep and doublet maneuvers injected into the pilot input as described in Ref. [1]. The aircraft was swept from 0.5 rad/s to 60 rad/s over 60 seconds while in hover in each axis. Each flight data log included 5 seconds of trim condition before and after the maneuver to allow for removal of sensor bias. The resulting flight data was then processed via a MATLAB script which performed unit conversion, data truncation, and processed the data to be compatible with the CIFER® software package. Fig. 2 shows sample pilot input, mixer input, and roll attitude for lateral sweep.

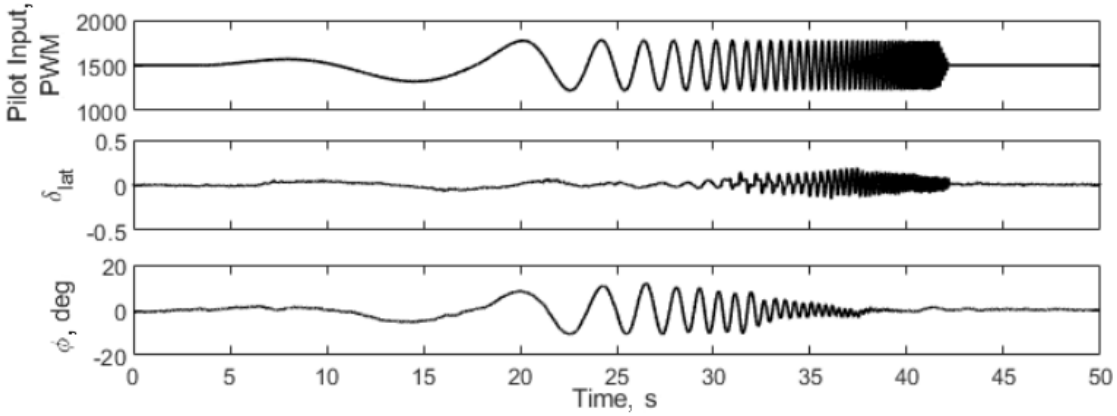

Fig. 2 Sample lateral frequency sweep data.

For the purposes of identification, actuator equivalent input to the bare airframe system was considered to be ArduCopter's internal motor mixer input signals. These signals are generated by the ArduCopter's control system and is used by the motor mixer to output signals to individual motors, allowing for easily referenced input that is unaffected by the configuration of the copter or the flight mode. Therefore, the *bare airframe dynamics* of the identified system includes the control mixer, motor response lag, vehicle dynamics, and the sensor dynamics. This is visualized in Fig. 3.

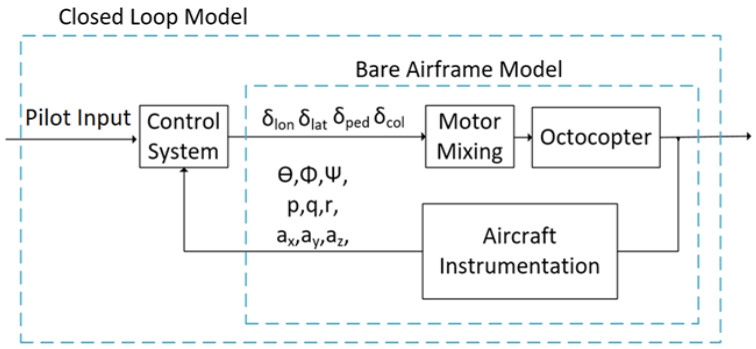

Fig. 3 Structure of bare airframe model.

The frequency responses of each axis were obtained from the frequency sweeps using CIFER®'s FRESPID module. Body translational accelerations were reconstructed via the following equations [1]:

$$\dot{u} = a_{x_{cg}} - W_0 q + V_0 r - (g \cos \Theta_0)\theta + b_x \tag{1}$$

$$\dot{v} = a_{y_{cg}} - U_0 q + W_0 p + (g \cos \Theta_0)\Phi + b_y \tag{2}$$

$$\dot{w} = a_{z_{cg}} - V_0 p + U_0 q - (g \sin \Theta_0)\theta + b_z \tag{3}$$

where b_x, b_y, and b_z are biases.

Through MISOSA and COMPOSITE modules of CIFER®, effects of cross-correlated inputs were removed, and composite windowing was performed to gain more accurate frequency responses across a wider frequency range [1]. A sample bare-airframe frequency response of p/δ_{lat} is shown in Fig. 4.

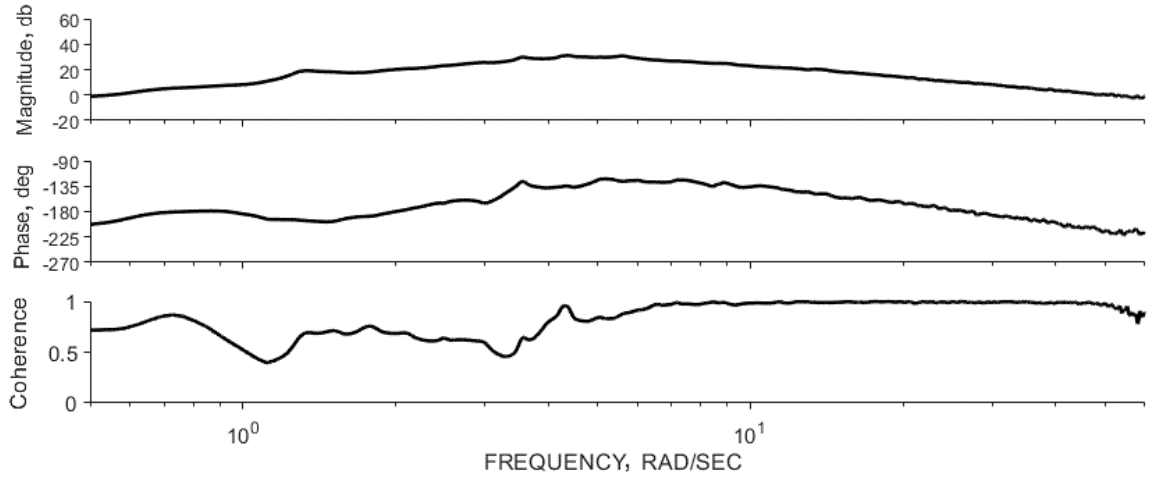

Fig. 4 p/δ_{lat} frequency response.

Coherence is high across most of the frequency range of interest, showing excellent linearity and high signal to noise ratio in the data.

The details of obtaining frequency responses via CIFER®, as well as the identification method that will be outlined below, are explained in depth in Ref. [1].

B. Transfer Function Model Identification

In order to obtain initial estimates of parameters for state-space model identification, lower-order transfer function models of vehicle dynamics were identified from the dominant on-axis frequency responses. This was accomplished using the NAVFIT module of CIFER®. The low order dynamics that were identified from the frequency responses chosen from previously identified multirotor dynamics [3] and are shown below.

$$\frac{p}{\delta_{\text{lat}}} = \frac{\text{L}_{\text{lat}}\, \text{s}\, (\text{s}-\text{Y}_\text{v})\, \text{e}^{-\tau_{lat}s}}{\text{s}^3-\text{Y}_\text{v}\text{s}^2-\text{L}_\text{v}\text{g}} \tag{4}$$

$$\frac{q}{\delta_{\text{lon}}} = \frac{\text{M}_{\text{lon}}\, \text{s}\, (\text{s}-\text{X}_\text{u})\, \text{e}^{-\tau_{lon}s}}{\text{s}^3-X_u\text{s}^2+\text{M}_\text{u}\text{g}} \tag{5}$$

$$\frac{a_z}{\delta_{col}} = Z_{col}\, \text{e}^{-\tau_{col}s} \tag{6}$$

$$\frac{r}{\delta_{ped}} = \frac{N_{ped}\, \text{e}^{-\tau_{ped}s}}{s-N_r} \tag{7}$$

The identification was performed in the frequency range of 0.5 – 15 rad/s. The cost function (J) of each individual model were all below 40 with exception of yaw axis, which had a cost function of 77.8. A comparison of the lateral input-to-roll rate transfer function model response and the flight data is shown in Fig. 5.

The high coherence and the low cost function indicate a good agreement of the transfer function model response with the flight data, and that the low order transfer models capture the flight dynamics fairly accurately. The transfer function model parameters were later used as initial starting values for the identification of the state-space model using the DERIVID module in CIFER®.

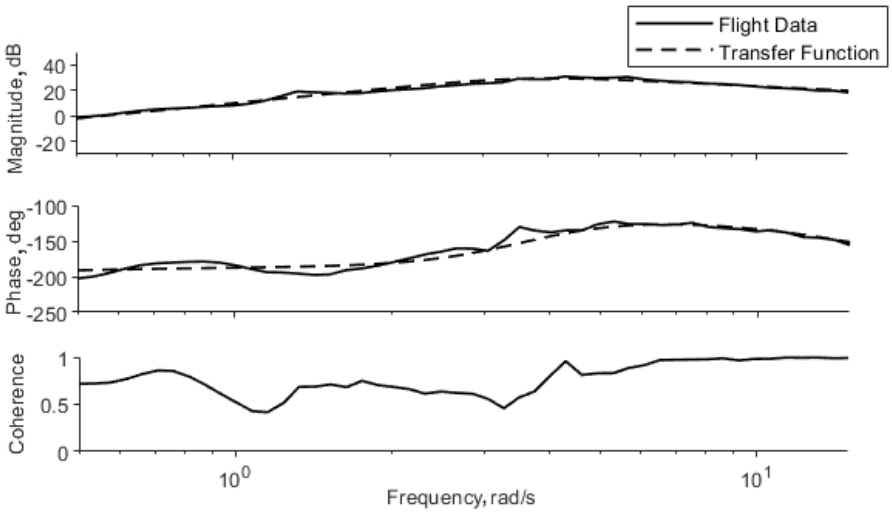

Fig. 5 p/δ_{lat} transfer function frequency response vs. flight data.

Below is a table summarizing the estimated parameter values obtained from transfer function model identification of the X8+.

Table 2 Identified transfer function model parameters of X8+.

Engineering Symbol	Value
Y_v	-0.0818
L_v	-1.436
L_{lat}	146.1
X_u	-0.301
M_u	-1.731
M_{lon}	138.0
Z_{col}	-81.5
N_{ped}	24.0
N_r	-0.9401

C. State-Space Model Identification

The state-space identification was accomplished using the DERIVID module of CIFER®. The module is capable of calculating insensitivity as well as Cramer-Rao bounds, adjusted to represent 1σ confidence interval. With the initial values of parameters identified via NAVFIT, a state-space model was identified from the frequency responses obtained above. Through elimination of parameters with high insensitivity or high Cramer-Rao bounds, the model was reduced until no extraneous parameters were left [1]. The model structure is based on the extensive quadrotor identification efforts in Ref. [3, 4].

To model the motor dynamics, and to correct the inadequacy of the identified model's yaw dynamics in the traditional state-space structure, the structure of the state-space model has been augmented. Four new states were added to represent "delayed" input in order to represent the motor dynamics [3] as shown in the below equation.

$$\frac{\delta input_{lag}}{\delta input} = \frac{lag}{s+lag} \tag{8}$$

In addition, additional yaw dynamics was added, as shown below.

$$\frac{\delta ped_{lag\_lead}}{\delta ped_{lag}} = \frac{lead*s+1}{N_{\delta ped}} \tag{9}$$

The final model structure is given below.

$$\begin{bmatrix} \dot{u} \\ \dot{v} \\ \dot{w} \\ \dot{p} \\ \dot{q} \\ \dot{r} \\ \dot{\theta} \\ \dot{\phi} \\ \dot{\psi} \\ \dot{\delta lat}_{lag} \\ \dot{\delta lon}_{lag} \\ \dot{\delta col}_{lag} \\ \dot{\delta ped}_{lag} \end{bmatrix} = \begin{bmatrix} X_u & 0 & 0 & 0 & 0 & 0 & -g & 0 & 0 & 0 & X_{\delta lon} & 0 & 0 \\ 0 & Y_v & 0 & 0 & 0 & 0 & 0 & g & 0 & Y_{\delta lat} & 0 & 0 & 0 \\ 0 & 0 & 0 & 0 & 0 & 0 & 0 & 0 & 0 & 0 & 0 & Z_{\delta col} & 0 \\ 0 & L_v & 0 & 0 & 0 & 0 & 0 & 0 & 0 & L_{\delta lat} & 0 & 0 & 0 \\ M_u & 0 & 0 & 0 & 0 & 0 & 0 & 0 & 0 & 0 & M_{\delta lon} & 0 & 0 \\ 0 & 0 & 0 & 0 & 0 & N_r & 0 & 0 & 0 & 0 & 0 & 0 & N_{\delta ped} - lag * lead \\ 0 & 0 & 0 & 0 & 1 & 0 & 0 & 0 & 0 & 0 & 0 & 0 & 0 \\ 0 & 0 & 0 & 1 & 0 & 0 & 0 & 0 & 0 & 0 & 0 & 0 & 0 \\ 0 & 0 & 0 & 0 & 0 & 1 & 0 & 0 & 0 & 0 & 0 & 0 & 0 \\ 0 & 0 & 0 & 0 & 0 & 0 & 0 & 0 & 0 & -lag & 0 & 0 & 0 \\ 0 & 0 & 0 & 0 & 0 & 0 & 0 & 0 & 0 & 0 & -lag & 0 & 0 \\ 0 & 0 & 0 & 0 & 0 & 0 & 0 & 0 & 0 & 0 & 0 & -lag & 0 \\ 0 & 0 & 0 & 0 & 0 & 0 & 0 & 0 & 0 & 0 & 0 & 0 & -lag \end{bmatrix} \begin{bmatrix} u \\ v \\ w \\ p \\ q \\ r \\ \theta \\ \phi \\ \psi \\ \delta lat_{lag} \\ \delta lon_{lag} \\ \delta col_{lag} \\ \delta ped_{lag} \end{bmatrix}$$

$$+ \begin{bmatrix} 0 & 0 & 0 & 0 \\ 0 & 0 & 0 & 0 \\ 0 & 0 & 0 & 0 \\ 0 & 0 & 0 & 0 \\ 0 & 0 & 0 & 0 \\ 0 & 0 & 0 & lag * lead \\ 0 & 0 & 0 & 0 \\ 0 & 0 & 0 & 0 \\ 0 & 0 & 0 & 0 \\ lag & 0 & 0 & 0 \\ 0 & lag & 0 & 0 \\ 0 & 0 & lag & 0 \\ 0 & 0 & 0 & lag \end{bmatrix} \begin{bmatrix} \delta lat(t - \tau_{lat}) \\ \delta lon(t - \tau_{lon}) \\ \delta col(t - \tau_{col}) \\ \delta ped(t - \tau_{ped}) \end{bmatrix}$$

$$\begin{bmatrix} \dot{u} \\ \dot{v} \\ p \\ q \\ r \\ \theta \\ \phi \\ \psi \\ a_x \\ a_y \\ a_z \end{bmatrix} = \begin{bmatrix} X_u & 0 & 0 & 0 & 0 & 0 & -g & 0 & 0 & 0 & X_{\delta lon} & 0 & 0 \\ 0 & Y_v & 0 & 0 & 0 & 0 & 0 & g & 0 & Y_{\delta lat} & 0 & 0 & 0 \\ 0 & 0 & 0 & 1 & 0 & 0 & 0 & 0 & 0 & 0 & 0 & 0 & 0 \\ 0 & 0 & 0 & 0 & 1 & 0 & 0 & 0 & 0 & 0 & 0 & 0 & 0 \\ 0 & 0 & 0 & 0 & 0 & 1 & 0 & 0 & 0 & 0 & 0 & 0 & 0 \\ 0 & 0 & 0 & 0 & 0 & 0 & 1 & 0 & 0 & 0 & 0 & 0 & 0 \\ 0 & 0 & 0 & 0 & 0 & 0 & 0 & 1 & 0 & 0 & 0 & 0 & 0 \\ 0 & 0 & 0 & 0 & 0 & 0 & 0 & 0 & 1 & 0 & 0 & 0 & 0 \\ X_u & 0 & 0 & 0 & 0 & 0 & 0 & 0 & 0 & 0 & X_{\delta lon} & 0 & 0 \\ 0 & Y_v & 0 & 0 & 0 & 0 & 0 & 0 & 0 & Y_{\delta lat} & 0 & 0 & 0 \\ 0 & 0 & 0 & 0 & 0 & 0 & 0 & 0 & 0 & 0 & 0 & Z_{\delta col} & 0 \end{bmatrix} \begin{bmatrix} u \\ v \\ w \\ p \\ q \\ r \\ \theta \\ \phi \\ \psi \\ \delta lat_{lag} \\ \delta lon_{lag} \\ \delta col_{lag} \\ \delta ped_{lag} \end{bmatrix} \tag{10}$$

Table 4 shows the identified model parameters along with the Cramer Rao bounds expressed in percentage of the identified value.

Table 4 Identified state-space model parameters of X8+.

Engineering Symbol	Value	CR %
X_u	-0.6112	5.324
M_u	1.912	5.166
$X_{\delta lon}$	-17.97	5.124
$M_{\delta lon}$	148.7	3.608
Y_v	-0.4277	6.437
L_v	-1.644	6.142
Y_{lat}	18.49	4.530
L_{lat}	157.3	3.339
N_r	-0.5392	22.68
N_{ped}	18.51	7.095
Z_{col}	-82.28	2.960
τ_{lon}	0.01718	11.00
τ_{lat}	0.01747	9.471
τ_{col}	0.01920	10.50
τ_{ped}	0.02915	26.05
Lag	-17.50	4.695
Lead	-3.169	8.649

As was found in Ref. [3, 4], the angular response is dominated by L_v and M_u derivatives and the contribution of traditional angular dampening (L_p, M_q) is negligible. The final cost function $J_{avg} \approx 44$. The low cost function and Cramer-Rao bounds indicate that the model is highly accurate and that the identified parameters are reliable. As shown in Fig. 6 and Fig. 7, the model response very closely follows the flight data.

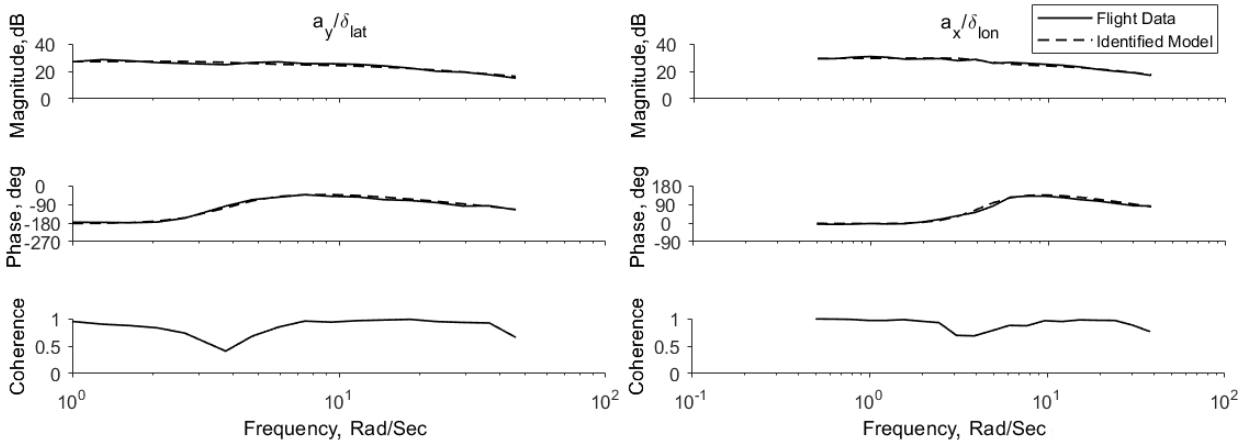

Fig. 6 Frequency-domain comparison of model response with flight data for lateral and forward accelerations.

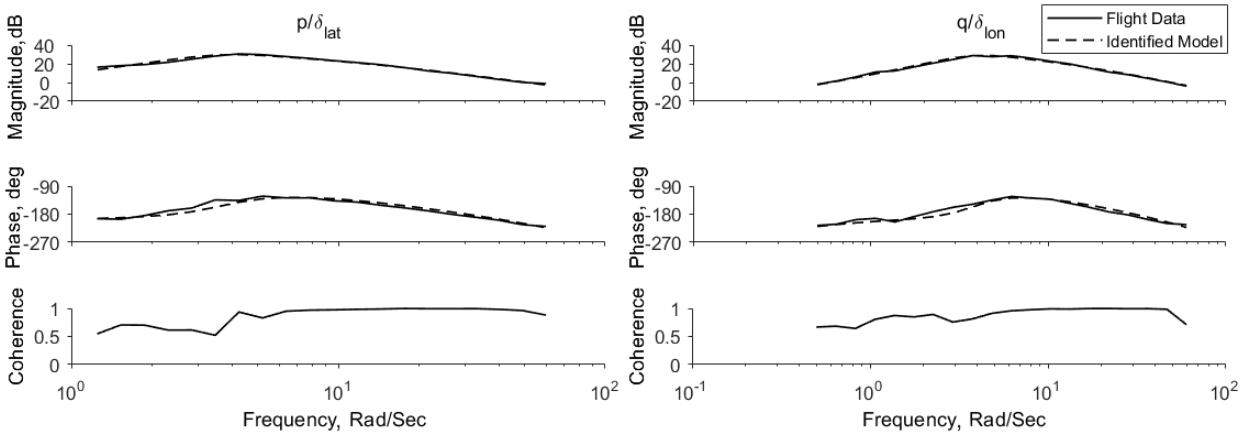

Fig. 7 Frequency-domain comparison of model response with flight data for roll and pitch rates.

D. Time-Domain Verification

As the model was identified entirely in the frequency domain, time domain verification via a different maneuver is necessary to ensure good predictive accuracy in the time domain. The time domain identification was accomplished via the VERIFY module of CIFER®, in which a flight test data of a doublet maneuver in each axis was used to verify the model. The VERIFY module is capable of identifying and compensating for sensor biases as well as drift [1]. The verification results for the lateral axis are shown in Fig. 8. The verification shows that the identified model is capable of tracking the flight test data closely, even in maneuvers where attitude reaches nonlinear ranges.

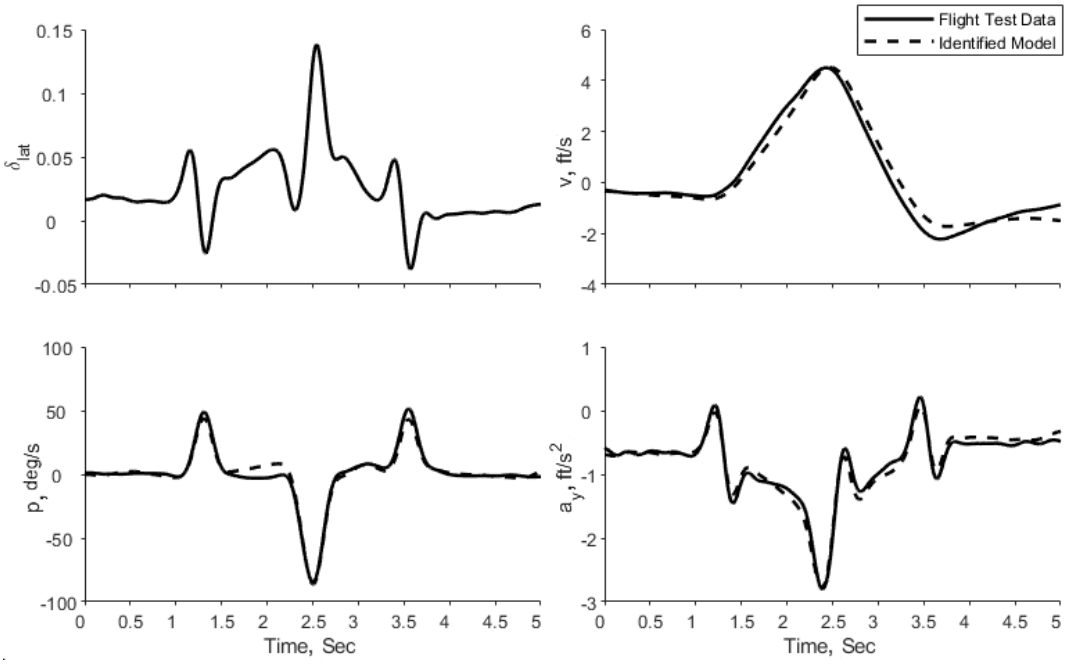

Fig. 8 Lateral axis verification results.

E. Comparison of Flight Dynamics

In order to assess the effect of coaxial configuration on the vehicle dynamics, the dynamics of the X8+ was compared with the dynamics of the 3DR IRIS+ [3], a multirotor in a standard quadrotor configuration with similar physical dimensions to the X8+.

Table 5 Comparison of hover dynamic modes of X8+ and IRIS+.

	X8+		IRIS+	
	ω (rad/s)	ζ	ω (rad/s)	ζ
Lon	3.90		3.93	
	3.68	-0.47	3.77	-0.48
Lat	4.16		2.65	
	3.84	-0.46	2.55	-0.48
Ped	0.54		0	
Motor	17.50		50 (fixed)	

As shown in Table 5, the dynamic modes of the coaxial X8+ and quadrotor IRIS+ in hover are nearly identical. While X8+ has more control power available due to its coaxial configuration, the configuration itself does not have a significant impact on the dynamic modes of the aircraft.

V. Control Law Design

The control law architecture chosen to design the optimized control system was Explicit Model Following (EMF) architecture. EMF is considered a "two degree of freedom" feedback system, where pilot command response characteristics can be designed separately from feedback response. The EMF architecture was chosen as it is widely used in many full-scale aircraft control systems [2]. A typical EMF architecture structure is shown below.

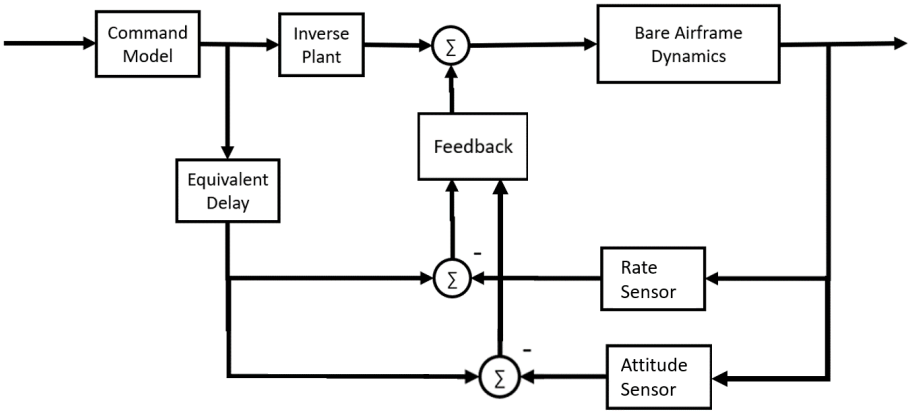

Fig. 9 EMF architecture.

In an EMF architecture, command model outputs a desired aircraft response from pilot input, and the inverse plant uses a lower order model of the bare airframe dynamics to generate a feed-forward control signal. Equivalent delay is used to synchronize the command model output with the feedback signal from the higher-order dynamics. The feedback loop is used for gust rejection, correction of any inverse plant errors, and ensure robustness [2].

The command response for the angular axes were chosen to provide Attitude Command/Attitude Hold (ACAH) [3]. The angular axes command models are show below:

$$\frac{\phi_{cm}}{\delta_{lat}}(s), \frac{\theta_{cm}}{\delta_{lon}}(s) = \frac{K_{lat\_cm}\omega_{cm}}{s^2+2\zeta\omega_{cm}s+{\omega_{cm}}^2} \tag{11}$$

Table 6 Lateral/ longitudinal command model parameters.

	Lat	Lon
Stick Gain (degrees/100%)	30	
Natural Frequency (rad/s)	6	
Damping Ratio	0.8	

The translation and yaw responses were selected as first order responses [2].

$$\frac{w_{cm}}{\delta_{col}}(s), \frac{r_{cm}}{\delta_{ped}}(s) = \frac{K_{cm}}{\tau_{cm}s + 1} \tag{12}$$

Table 7 Collective/pedal command model parameters.

	Col	Ped
Stick Gain (ft/s/100%, degrees/100%)	3	90
Time Constant (τ)	1/6	

Inverse plants were obtained by rearranging the low order transfer function models from Eqs. (4-7) to produce actuator signal as a function of aircraft attitude. The inverse plant for each axis is as follows, with parameters taken directly from the identified model above:

$$\delta_{lat_{ff}} = (\dot{p}_{cm} - \frac{L_v g}{s - Y_v}\Phi_{cm})/L_{lat} \tag{13}$$

$$\delta_{lon_{ff}} = (\dot{q}_{cm} + \frac{M_u g}{s - X_u}\theta_{cm})/M_{lon} \tag{14}$$

$$\delta_{col_{ff}} = a_{z_{cm}}/Z_{col} \tag{15}$$

$$\delta_{ped_{ff}} = \frac{\dot{r}_{cm} - N_r r_{cm}}{N_{ped}} * \frac{N_{ped}}{lead * s + 1} \tag{16}$$

The motor dynamics was not included in the inverse plant due to the fact that it would command large, high-frequency inputs which is not desirable [2].

Equivalent delays were identified by modeling the ratio of the bare airframe model output to command model output as simple delays ($e^{-\tau s}$). The identified delays are shown in Table 8:

Table 8 Identified equivalent delays.

Lat	Lon	Col	Ped
0.0632s	0.0615s	0.0703s	0.1306s

VI. Optimization of Control Law

Optimization of the control law was accomplished using the CONDUIT® software package. CONDUIT® optimizes a given set of design parameters against a set of handling quality "specs," or specifications plots derived from various requirements such as ADS-33. Handling quality specs provided by the built in libraries were utilized, with crossover frequency specs and disturbance rejection specs modified based on the specs used for the optimization of the IRIS+. Each spec was then assigned a constraint type, which indicated the priority of meeting Level 1 handling quality requirements: hard, soft, and objective. Objective specs are optimized last to achieve all of the specs with minimum overdesign, reaching the Pareto Optimum [2]. When optimizing, CONDUIT® plots the design on the Handling Qualities Window (HQ Window), calculating its performance based on the distance between the handling quality Level boundaries. By driving the design towards the Level 1 boundary, the control system is driven to fulfill all Level 1 handling qualities. The optimization specifications then drive the design towards the Pareto optimum.

The primary objective of optimization was reduction in actuator usage. In addition, the integrator gains were fixed to be 2/5th of the proportional gain, as the optimization process can deem the integrator gains to be insensitive and drive them to undesirable values. For this optimization, minimum crossover frequency of 20 rad/s was chosen. The CONDUIT® specifications used are listed in Table 9.

Table 9 CONDUIT® specs used.

CONDUIT® Spec	Description	Constraint
EigLcG1	Eigenvalues	Hard
NicMgG1	Nichols Plot Margin for Robust Stability	Hard
StbMgG1	Stability and Gain Margin	Hard
CrsMnG2	Minimum Crossover Frequency	Soft
DrbRoX1	Disturbance Rejection Bandwidth	Soft
DrpAvH1	Disturbance Rejection Peak	Soft
ModFoG2	Model Following Response Comparison Cost	Soft
RmsAcG1	Actuator RMS	Objective
CrsLnG1	Crossover Frequency	Objective

As the initial control system was unable to meet the Level 1 handling guidelines, lead-lag compensators were added to the feedback of longitudinal and lateral axes, and a lead compensator was added to the heave and yaw feedback control. The parameters were selected through iterations of optimization. The parameters of the compensators are shown in the equations below:

$$\text{Longitudinal, Lateral Axis:} \quad \frac{(s+3)(s+4)}{(s+72)(s+0.1)} \tag{17}$$

$$\text{Collective Axis:} \quad \frac{s+3}{s+48} \tag{18}$$

$$\text{Directional Axis:} \quad \frac{s+10}{s+24} \tag{19}$$

After optimization by CONDUIT®, the HQ Window of the optimized solution is shown in Fig. 10. Many of the specifications have the design points on the border of Level 1 (shown in blue) and Level 2 (shown in magenta), indicating that the optimization has driven the design to its Pareto optimum. The optimized gains are shown in Table 10.

Table 10 Optimized gains.

K_p	0.610	K_Φ	7.274
K_q	0.643	K_θ	7.603
K_w	0.979	K_z	11.47
K_r	0.329	K_ψ	11.17

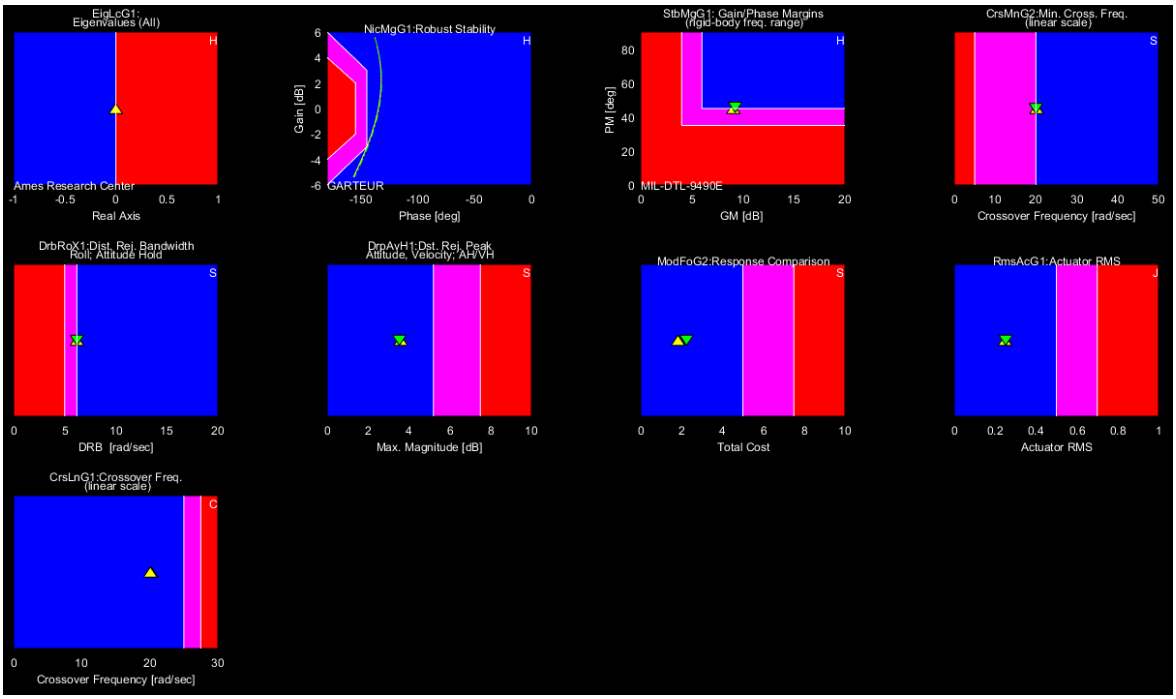

a) HQ Window for optimized longitudinal (yellow) and lateral (green) axes.

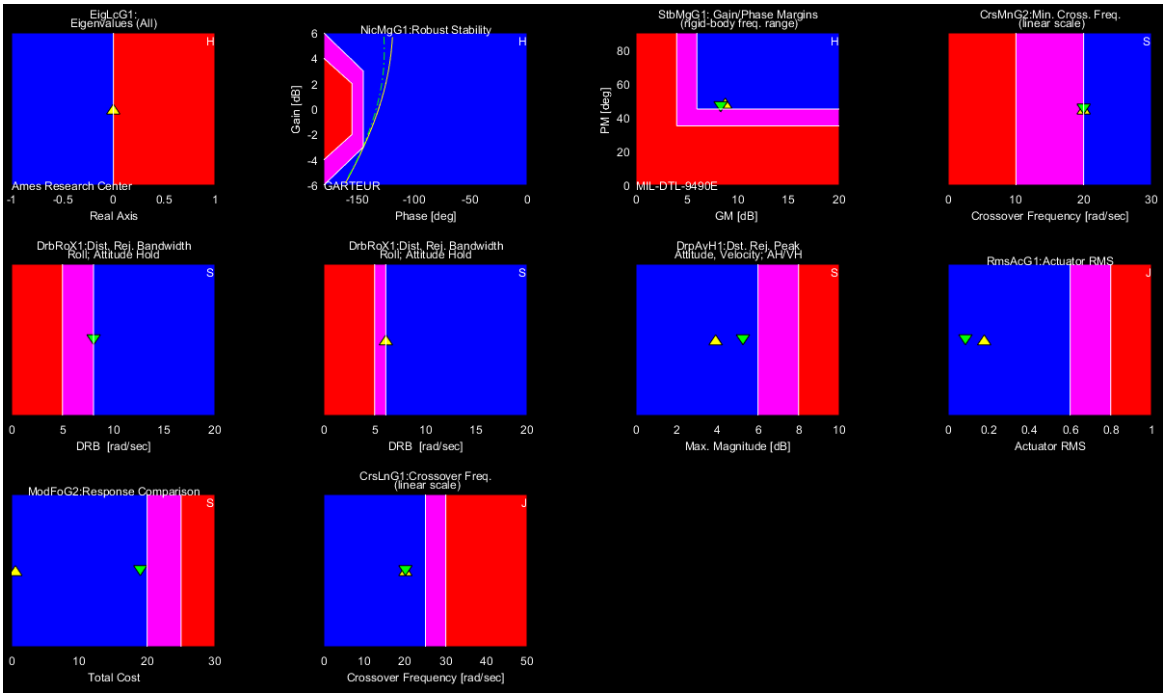

b) HQ Window for optimized collective (yellow) and directional (green) axes.

Fig. 10 HQ Window of optimized system.

Figure 11 shows the system response to a unit step pilot lateral input. As shown, the control system is capable of tracking the command model closely. Figure 12 shows a 15 degree gust impulse response, and lateral axis broken loop response is shown in Fig. 13.

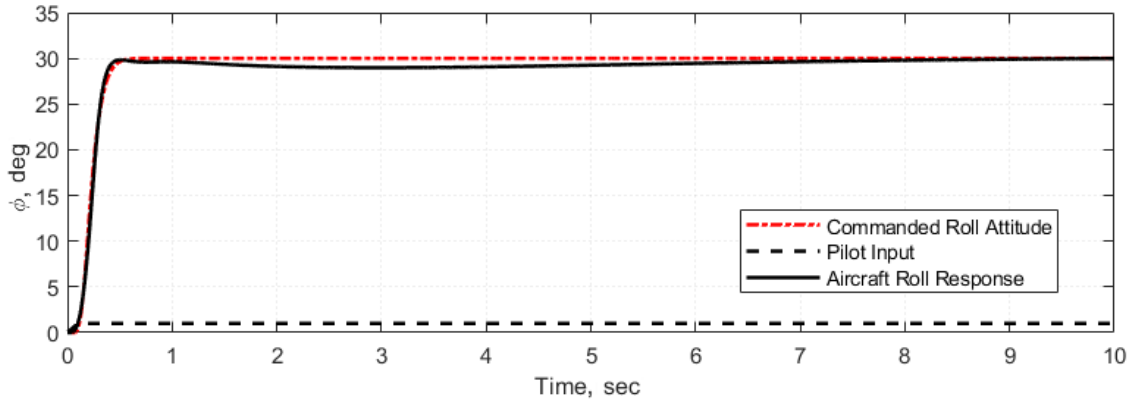

Fig. 11 Lateral axis pilot step response.

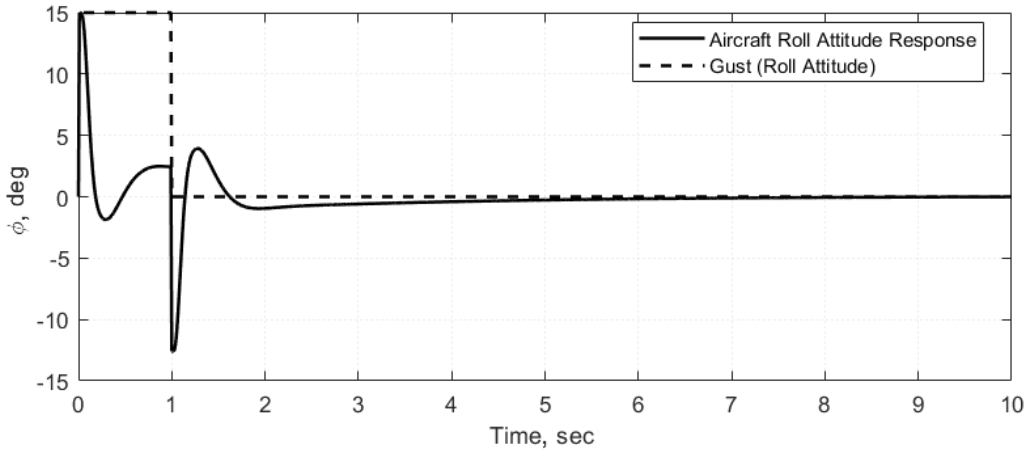

Fig. 12 Roll axis gust impulse response.

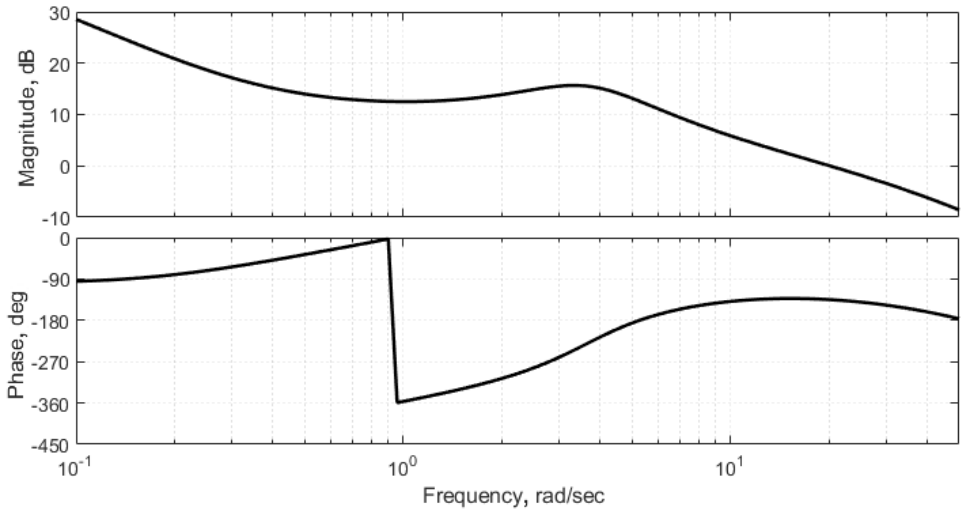

Fig. 13 Lateral axis broken loop response.

F. Comparison of Control Laws

To identify any effect of the coaxial configuration on the design and optimization process, the optimized performance of X8+ control laws was compared with the performance of the optimized control laws for IRIS+. Control laws for IRIS+ was optimized in a similar method using EMF and utilizing disturbance rejection bandwidth

as its primary performance parameter. Comparison of the optimization of the X8+ and the IRIS+ was performed by comparing major performance parameters of minimum crossover frequency, disturbance rejection bandwidth, and phase and gain margins. The performance parameters of the X8+ was taken from the lateral axis.

Table 11 Comparison of optimized IRIS+ and X8+ control system.

Vehicle	Phase Margin (deg)	Gain Margin (dB)	DRB (rad/s)	Crossover Freq. (rad/s)
X8+	45	8.3	6.1	20
IRIS+ [3]	42	11.2	10.2	31.6

As shown, the difference in the designs is not significant; the difference in the disturbance rejection bandwidth most likely can be attributed to the relaxed phase margin requirement of the IRIS+ and the higher minimum crossover frequency that was enforced.

VII. Conclusion and Future Work

The 3DR X8+'s hover/low-speed bare airframe dynamics was identified using the CIFER® software package. The identified model was shown to be accurate to the frequency range of 0.5 – 60 rad/s, and the accuracy of the model was verified in the time domain using a doublet flight data. The identified model's angular response is dominated by L_v and M_u derivatives, with traditional angular damping derivatives having negligible contribution to the dynamics. From comparison of the identified dynamic modes and the model structure to the previously identified IRIS+, it was concluded that the coaxial configuration has little to no effect on the hover/low-speed dynamics of a quadrotor.

The X8+'s bare airframe dynamics was then utilized to design and optimize an Attitude Command/Attitude Hold control system using the Explicit Model Following architecture. Optimization was conducted via the CONDUIT® software package, which optimized the control system to its Pareto optimum via reducing actuator usage while retaining Level 1 handling qualities defined by the handling quality specs.

Future work would entail design and optimization of a velocity hold and position hold outer loops of the X8+ control system, and flight testing of the control system. In addition, a forward flight model will be identified and verified. The verified model will then be used for the design and optimization of control laws for forward flight.

References

[1] Tischler, M. B., and Remple, R., "Aircraft and Rotorcraft System Identification, Second Edition," *American Institute of Aeronautics and Astronautics*, Aug 2012.

[2] Tischler, M. B., Berger, T., Ivler, C. M., et al., "Practical Methods for Aircraft and Rotorcraft Design: An Optimization-Based Approach," *American Institute of Aeronautics and Astronautics*, April 2017

[3] Cheung, K. K., Tischler, M. B., Wagster IV, J. A., "An Overview of the U.S. Army Aviation Development Directorate Quadrotor Guidance, Navigation, and Control Project," *Vertical Flight Society Forum 73*, May 2017

[4] Wei W., Tischler, M. B., and Cohen K., "System Identification and Controller Optimization of a Quadrotor Unmanned Aerial Vehicle in Hover," *Journal of the American Helicopter Society 62*, 2017.